25th ABCM International Congress of Mechanical Engineering
October 20-25, 2019, Uberlândia, MG, Brazil

N-th Order Unified Formulation Model for Rotordynamics

Vergílio T. S. Del Claro[1,2], Aldemir A. Cavalini Junior[1], Ilmar F. Santos[2], and Valder Steffen Jr.[1]
vergilio.claro@ufu.br, aacjunior@ufu.br, ifs@mek.dtu.dk and vsteffen@ufu.br
1 - Federal University of Uberlandia, LMEst - Structural Mechanics Laboratory, Av. João Naves de Ávila, 2121, Block 1O Uberlândia, MG, CEP 38408-196, Brazil; 2 - DTU Mekanik – Denmark Technical University, Mechanics Department, Nils Koppels Allé, DTU Building 404, Office 005, 2800 Kongens Lyngby, Denmark

Abstract. *The design of rotating machines greatly evolved in the last five decades, as aided by advanced computational models, which are able to describe new material properties and the dynamic behavior of elements with complex geometry at high rotational speeds. To foster this field of research, a Unified Formulation Finite Element Model specifically developed for rotordynamics is presented. In a Unified Formulation numeric model, the number of nodal degrees of freedom and the order and type of interpolation functions are arbitrary. The goal of this novel technique is to produce physically coherent results for rotating elements for any given geometry and material properties, by using Nth order polynomial interpolations and N_nth order beam elements. The model is also able to represent any cross-section geometry and orthotropic materials, producing 3D-like solutions. To keep the computational cost affordable, unimportant terms can be identified and neglected in the formulation, yielding precise results at a fraction of the cost. In this publication, a proof of concept case-study is carried out by simulating a composite-shaft rotor with Timoshenko, 1st, 2nd and 3rd order Taylor-like polynomial interpolations, with two-node beam elements. The present theoretical analysis shows good qualitative results, and an increasingly realistic dynamic behavior for higher order models.*

Keywords: *Unified Formulation, Rotordynamics, Finite Element Method*

1. INTRODUCTION

A major advancement in rotordynamics came out with the use of composite shafts, since they overcome intrinsic limitations of metallic ones (Silveira, 2001). The low weight of composites allows for faster acceleration and deceleration as compared to conventional rotating machines (Brush, 1999), and also reduces effects related to rotational inertia. An unfortunate side-effect however, is that composites have a more complex behavior as compared with isotropic materials. Besides, in supercritical operations the vibration responses demand special attention (Gupta, 2015) to ensure a safe operation (Del Claro *et al.*, 2017), (Sino *et al.*, 2008). Nevertheless, it is possible to change the stiffness and damping properties by manipulating some characteristics on the model (Barbosa *et al.*, 2018). Additionally, it is possible to attenuate the vibration amplitudes when the system undergoes critical speeds, depending on the structural damping properties of the composite (Mendonça *et al.*, 2017), which significantly influences the system dynamic response (Bucciarelli, 1982), (Wasilkoski, 2006).

Another arising challenge is the modeling of complex rotating geometries, such as thick-walled shafts and flywheels, operating at above-critical speeds (Carrera and Filippi, 2015). These systems demand high order models to accurately represent the stress-strain relations of the moving structure. Considering their geometry, material property and wall thickness requirements, simplified models are unsuited for obtaining accurate results for this type of application (Barbosa *et al.*, 2019). These complexities have pushed the development of new and modified models, featuring improved physical representation of the real systems. Different Finite Elements Method (FEM) formulations based on the homogeneous beam theory, equivalent layer theories and layerwise models, have been recently proposed for the analysis of composite materials by a number of authors.

Nevertheless, when numerical models are used, a compromise solution is generally proposed, aiming at balancing the accuracy of the results with model complexity and computational cost. As a general rule, the goal is to have sufficiently accurate models while keeping the computational cost low enough for the problem to be solvable. Considering recent models, aiming to give better results than traditional representations, such as Euler-Bernoulli and Timoshenko - the Classical Beam Theories (CBT) - a few examples can be cited. The Equivalent Modulus Beam Theory (EMBT) (Tsai, 1998), such as the one shown by (Singh and Gupta, 1996), can be effectively used for the modeling of tubular composite shafts, and can be even extended to represent rotating dynamics accordingly, with a few limitations (Gubran and Gupta, 2005). A Layerwise Beam Theory (LBT) (Singh and Gupta, 1996) presents an excellent prediction of the composite shaft dynamics in rotating machine applications, but leads to an exponentially higher computational cost (Carrera *et al.*, 2014), depending on the number of layers considered. An intermediary approach was studied, resulting on a modified version of the EMBT (Barbosa *et al.*, 2018) models, and also on the Simplified Homogenized Beam Theory (SHBT) (Sino, 2007). An Unified Formulation (UF) was presented by Carrera (CUF), bringing a methodology to determine the “best theory”

for a given problem (Carrera *et al.*, 2011). Alternate solutions, such as the Rayleigh-Ritz method, were also recently used for composite shafts (Cavalini Jr. *et al.*, 2017).

To foster the understanding of composite thick-walled shaft rotors, the authors present a N-th order UF FEM model, with extended damping and orthotropic material considerations. A SHBT can be applied to composite materials, providing accurate results for thin to moderately thick walls, while maintaining the computational cost acceptable. Otherwise, a full LBT model can be selected, if the application demands, providing reliable results at a higher cost. This model enables the determination of 3D-like solutions for rotating machinery problems, being limited only by the boundary conditions representation and computational power. The model assumptions and general formulation is presented in the next session, featuring a proof of concept by modeling a thick-walled composite-shaft rotor, similar to the overhung configuration (Friswell *et al.*, 2010), (Barbosa *et al.*, 2019).

2. UNIFIED FORMULATION

The UF utilized in this model is based on the works of (Carrera *et al.*, 2011), (Carrera *et al.*, 2014) and (Filippi, 2015), featuring a number of modifications and added functionalities. By maintaining the interpolation order and element type as input parameters, this method is not restricted to the limitations of standard theories and produces very accurate and easily adaptable structural models. The displacement field interpolation functions are also arbitrarily chosen, and no assumption about them is made beforehand. Regarding the orthotropic composite formulation and internal material damping properties, an equivalent layer integration (SHBT) (Barbosa *et al.*, 2019) and a Kelvin-Voigt rheological model (Sino, 2007) are respectively used. The effect of transient stiffening during acceleration has also been included.

2.1 Interpolation functions, material and geometry modeling

The model construction begins by defining the nodal displacement vector as in Eq. (1),

$$u(x,y,z) = \{u_x, u_y, u_z\}^T, \ where \ \ 0 \leqslant y \leqslant L \tag{1}$$

where L is the shaft length in the y direction and the x, z plane defines the cross-section geometry. Material properties are dependent on the fibers angle relative to the shaft axis (Cavalini Jr. *et al.*, 2017), for each ply. As it has been proven by previous works using ESL theories, a shaft with wall to radius ratio smaller than 30% (moderately thick) can be modeled by SHBT or EMBT with satisfactory results (Del Claro *et al.*, 2017). Next, one can define the time dependent vector $u(x,y,z)$ as in Eq. (2):

$$u(x,y,z,t) = F_\tau(x,z)u_\tau(y,t), \quad \tau = 1, 2, \cdots, N \tag{2}$$

expressing the cross-section interpolation by F_τ, Eq. (4), and the displacement vector is given by u_τ. The τ sub-index indicates Einstein summation notation. This yields the u_i $(i = x, y, z)$ terms of Eq. (3):

$$\begin{cases} 0th \ order \Rightarrow u_i = F_1 u_{i1} \\ 1st \ order \Rightarrow u_i = \{0th\} + F_2 u_{i2} + F_3 u_{i3} \\ 2nd \ order \Rightarrow u_i = \{1st\} + F_4 u_{i4} + F_5 u_{i5} + F_6 u_{i6} \\ 3rd \ order \Rightarrow u_i = \{2nd\} + F_7 u_{i7} + F_8 u_{i8} + F_9 u_{i9} + F_{10} u_{i10} \\ \cdots \\ Nth \ order \Rightarrow u_i = \{\cdots\} + F_{(N^2+N+2)/2} u_{i(N+1)} + \cdots + F_M u_{iM} \end{cases} \tag{3}$$

$$\begin{cases} 0th \ order \Rightarrow F_1 = 1; \\ 1st \ order \Rightarrow F_2 = x; \ F_3 = z; \\ 2nd \ order \Rightarrow F_4 = x^2; \ F_5 = xz; \ F_6 = z^2; \\ 3rd \ order \Rightarrow F_7 = x^3; \ F_8 = x^2 z; \ F_9 = xz^2; \ F_{10} = z^3; \\ \cdots \\ Nth \ order \Rightarrow F_{(N^2+N+2)/2} = x^N; \ \{\cdots\}; \ F_M = z^N. \end{cases} \tag{4}$$

where N is the interpolation order and M is the amount of generalized Degrees of Freedom (DoFs) per node, given by $M = (1/2)(N+1)(N+2)$. Making an analogy to the CBT, specifically to the Timoshenko model (Zienkiewicz and Taylor, 2005), u_{x1} and u_{z1} are equivalent to the translational DoFs x and z, while u_{y2} and u_{y3} the rotational DoFs θ and φ, respectively. Degenerating the UF into any classical model is a simple matter of neglecting unimportant terms. For this Two Nodes Beam Element (B2), a simple interpolation is adopted in the longitudinal direction, such as explained by Eqs. (5) and (6).

$$u_\tau(y,t) = N_i(y) q_i(t), \ where \ \ q_i(t) = \{q_{ux\tau_i}, \ q_{uy\tau_i}, \ q_{uz\tau_i}\}^T, \ i = 1, \cdots, N_{nodes} \tag{5}$$

$$\begin{cases} N_1 = 1/2 * (1 - r); \\ N_2 = 1/2 * (r + 1); \\ r = \{-1,\ 1\}^T,\ for\ a\ B2\ element. \end{cases} \tag{6}$$

As the number of nodes per element in the longitudinal direction increases, so does the interpolation functions Ni increase in number and complexity. An element with 3 nodes, named B3, would have a parabolic interpolation function, a B4 would be cubic and so on, while a simple B2 element has a linear interpolation. Although in this formulation no limitations have been imposed for the element order, the B2 elements are generally adequate for long shafts such as the one considered here, while higher order interpolations are recommended for thick-walls, flywheels or high diameter elements, depending on the dynamics of the problem (Carrera *et al.*, 2014). By making use of high order elements, shell deformations and vibration modes are visible in thin walled hollow shafts. These effects start to appear with B4 beam elements, and improve in precision by using even higher orders, allowing to produce accurate shell-like deformation results at a low cost, when compared to a full shell FEM model.

2.2 Fundamental Nuclei assembly procedure

Another particularity of the UF is its assembly procedure. On a standard FEM model, the element type, interpolation functions and DoFs per node are defined from the start, while here that is not the case, and a generalized assembling technique is needed. This implies the definition of each individual term of the Stiffness, Damping and Mass matrices as dependent of four sub-indexes, leading to the matrix assembly along four loops to cover all the combinations.

In this procedure, the generalized "core" of each matrix, denominated *Fundamental Nuclei* (FN), consists of a 3x3 matrix, such as in Eq. (7). The formulation follows the Principle of Virtual Displacements (PVD), first determining the stress σ and strain ϵ components, later manipulating them to obtain each term of the FN. These are then introduced into two loops to form the nodal level matrices, which depend on the cross-section interpolation functions order, given by indexes τ and s, ranging from 1 to M. After that, the Element level matrices are assembled also using two loops, covering the indexes i and j, that represent the longitudinal interpolation dependent on the number of nodes per element, ranging from 1 to N_n. These last couple of assemblies are presented in Eqs. (8) and (9), where $\mathbf{b}$ is a differential operator matrix and $\mathbf{C}$ is the material coefficients matrix, which are calculated through SHBT layer integration for transversely orthotropic composite materials.

$$\begin{cases} \mathbf{k}^{\tau sij} = \int_V F_s(x,z) N_j(y) \mathbf{b}^T \mathbf{C} \mathbf{b} N_i(y) F_\tau(x,z) dV = \underbrace{\begin{bmatrix} k_{xx} & k_{xy} & k_{xz} \\ k_{yx} & k_{yy} & k_{yz} \\ k_{zx} & k_{zy} & k_{zz} \end{bmatrix}}_{(\mathbf{3x3});} \implies FN \\ Where:\ \mathbf{b} = \begin{bmatrix} \partial/\partial x & 0 & 0 \\ 0 & \partial/\partial y & 0 \\ 0 & 0 & \partial/\partial z \\ \partial/\partial z & 0 & \partial/\partial x \\ 0 & \partial/\partial z & \partial/\partial y \\ \partial/\partial y & \partial/\partial x & 0 \end{bmatrix},\ and\ \mathbf{C} = \begin{bmatrix} C_{11} & C_{12} & C_{13} & 0 & 0 & 0 \\ C_{21} & C_{22} & C_{23} & 0 & 0 & 0 \\ C_{31} & C_{32} & C_{33} & 0 & 0 & 0 \\ 0 & 0 & 0 & C_{44} & C_{45} & 0 \\ 0 & 0 & 0 & C_{54} & C_{55} & 0 \\ 0 & 0 & 0 & 0 & 0 & C_{66} \end{bmatrix} \end{cases} \tag{7}$$

$$\mathbf{k}^{ij} = \underbrace{\begin{bmatrix} \mathbf{k}^{11ij} & \mathbf{k}^{21ij} & \dots & \mathbf{k}^{M1ij} \\ \mathbf{k}^{12ij} & \mathbf{k}^{22ij} & \dots & \mathbf{k}^{M2ij} \\ \vdots & \vdots & \mathbf{k}^{\tau sij} & \vdots \\ \mathbf{k}^{1Mij} & \mathbf{k}^{2Mij} & \dots & \mathbf{k}^{MMij} \end{bmatrix}}_{(\mathbf{3Mx3M});\ \ \mathbf{Indexes\ \tau,s}} \implies Nodal\ Level \tag{8}$$

$$\mathbf{k}_{el} = \underbrace{\begin{bmatrix} \mathbf{k}^{11} & \mathbf{k}^{21} & \dots & \mathbf{k}^{N_n 1} \\ \mathbf{k}^{12} & \mathbf{k}^{22} & \dots & \mathbf{k}^{N_n 2} \\ \vdots & \vdots & \mathbf{k}^{ij} & \vdots \\ \mathbf{k}^{1N_n} & \mathbf{k}^{2N_n} & \dots & \mathbf{k}^{N_n N_n} \end{bmatrix}}_{(\mathbf{3MN_nx3MN_n});\ \ \mathbf{Indexes\ i,j}} \implies Element\ Level \tag{9}$$

Finally, the assembling for global level matrices follows the standard practice, depending on the number of elements adopted for a given problem mesh. Transfer and Connectivity matrices are used as usual, although they demand a similar generalized approach for their construction, as they also depend on the order of the interpolation functions and on the number of nodes per element. This technique presented here is extended for the assembling of all other matrices, such as

Gyroscopic, Damping, Mass matrix, and others. The matrices are assembled based on their physical origin, resulting in the Stiffness, Damping and Mass matrices being split into a number of sub-components. These are all individually built just as the classical stiffness matrix of the shaft $\mathbf{k}_{el}$, and follow the same assembling technique.

2.3 Constraints, forces and localized components

As a brief sidenote, terms such as localized forces, constraints and other elements with local influence are introduced directly at the adequate DoF or as nodal level matrices. For punctual forces, bearing supports and external constraints in general, the implementation consists in identifying the DoF(s) subject to their influence and adding them either directly (forces, bearings, local springs or dampers, etc.) or via penalty factor (in the case of a clamped DoF). For localized elements, such as disks and blades, the procedure is so that either a thick beam element with proper radius and higher order of interpolation on that particular element is added, or by creating a set of nodal level matrices specifically for the disks, and by subsequently adding them to their global level associated matrices. In this contribution, the bearings are applied as localized terms, directly at their corresponding DoFs, the gravity force is added to every node in the vertical direction, and the disks have their own set of nodal level matrices, which are added to the Global matrices during their assembling procedure.

3. ROTOR MODEL

Assembling the additional FEM model terms via Lagrange formulation, one can proceed according to the standard manner, separating the terms into Potential (U) and Kinetic Energies (T), equivalent to the work of non-conservative forces (W_{nc}) (Meirovitch, 1980). This formulation is developed so that the rotating dynamics, internal material damping, dynamic stiffening due to acceleration, gravity, *etc.* are included, as presented by Eq. (10):

$$\int_0^{t_f} \delta(T-U)dt + \int_0^{t_f} \delta W_{nc} dt \;\; \Rightarrow \delta \int_0^{t_f} (T-(U+U_{\sigma_0})+W_b)dt = 0 \tag{10}$$

being U_{σ_0} the energy associated with the wall deformation due to centrifugal effect and W_b the energy stored and dissipated by the bearings forces. By carrying out the Lagrange formulation, one can derive the Equation of Motion and generate each individual FEM matrix just as exemplified by the shaft stiffness matrix $\mathbf{k}_{el}$. For the sake of brevity, this model presents no forces other than the gravity and internal ones, originated by the shaft rotation and unbalanced masses. The Equation of Motion is presented according to the individual matrices separated by their physical origin, as given by Eq. (11),

$$[\mathbf{M}+\mathbf{M_d}]\ddot{q}+[\mathbf{C}+\mathbf{C_b}+\Omega(\mathbf{G}+\mathbf{G_d})]\dot{q}+[\mathbf{K}+\mathbf{K_b}+\mathbf{K_d}+\mathbf{Ks}+\mathbf{Ks_d}+\Omega^2(\mathbf{Ko}+\mathbf{Ko_d})+\mathbf{Kt}]q = \mathbf{W}+\mathbf{F_{unb}} \tag{11}$$

where $\mathbf{M}$ stands for mass, $\mathbf{C}$ for damping, $\mathbf{G}$ for gyroscopic and coriolis and $\mathbf{K}$ to stiffness matrices. The index $\mathbf{s}$ indicates the centrifugal effect, $\mathbf{o}$ dynamic stiffening and pre-stress, while $\mathbf{t}$ stands for motor torque. The additional sub-indexes $_\mathbf{d}$ and $_\mathbf{b}$ indicates the association with disks or bearings physical influences respectively. It is noteworthy that this specific formulation included the additional terms $\mathbf{C}+\mathbf{C_b}$ due to internal composite damping, obtained via Kelvin-Voight rheological model (Cavalini Jr. *et al.*, 2017). It also presents $\Omega^2(\mathbf{Ko}+\mathbf{Ko_d})$ due to dynamic stiffening effects under acceleration/deceleration conditions. In addition, the gravity effect on the structure own weight is added by $\mathbf{W}$ and the unbalanced forces by $\mathbf{F_{unb}}$. The material properties were obtained for an equivalent layer by means of a degenerated shell theory, as presented by the SHBT method (Sino, 2007).

4. NUMERICAL MODEL

For exemplifying the UF FEM model described above, a numerical exercise is proposed. A composite shaft rotor, similar to the overhung configuration proposed by (Friswell *et al.*, 2010) is modeled by 39 B2 elements, with cross-section interpolation functions of 1st, 2nd, 3rd orders and also by a Timoshenko model, obtained by neglecting the extra terms from the complete 1st order UF model. The setup is composed by a horizontal composite hollow shaft, two aluminum disks, and two self-aligning ball bearings, as seen in Fig. 1. The system displacement response is produced on the disks nodes, along the horizontal and vertical directions. The composite shaft used is made of carbon fibers into an epoxy resin

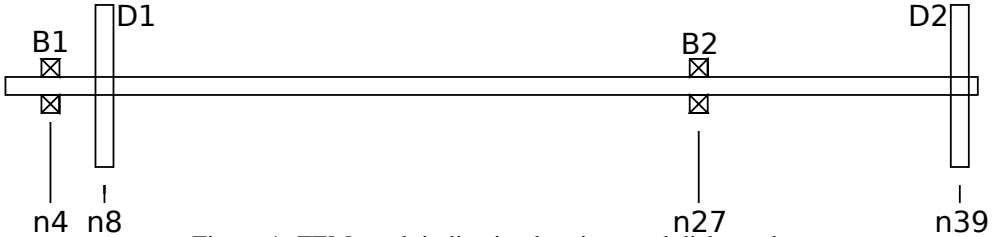

Figure 1: FEM mesh indicating bearings and disks nodes

matrix, presenting twenty layers with the following stacking sequence: [0, 0, 0, 0, 90, 90, 45, -45, 0, 0, 0, 45, -45, 90, 90, 0, 0, 0, 0, 0/90] (θ_k for each layer). The length is $907mm$, the external diameter $18mm$ and the internal $12.8mm$, while the volumetric density is $1667kg/m^3$. The Young's modulus along the fibers direction is $E1 = E3 = 1 \cdot 10^{11}Pa$ and in the transversal $E2 = 4.7 \cdot 10^{10}Pa$, while the shear modulus is $G = 9 \cdot 10^8 Pa$ for all directions, and the Poisson module is $\nu_{12} = 0.30$. This specific shaft was adopted due to its layers complexity and wall thickness, which is adequate to test the UF model. The disks are manufactured in aluminium, with a volumetric density of $2700kg/m^3$, thickness of $15mm$ and diameter of $150mm$. The bearings have values of stiffness $K^1_{xx} = K^1_{zz} = 1 \cdot 10^{10}N/m$ for the first disk and $K^2_{xx} = K^2_{zz} = 1 \cdot 10^9 N/m$ for the second, while the damping is $C^1_{xx} = C^1_{zz} = 1 \cdot 10^7 (NKg/m)^{1/2}$ for the first disk and $C^2_{xx} = C^2_{zz} = 1 \cdot 10^6 (NKg/m)^{1/2}$ for the second. The excitation forces for the simulations come from the unbalanced masses, weighting $10g$ for the first disk and $20g$ for the second, located at a radius of $75mm$, with phase of 5.945 and $5.257 radians$ respectively.

5. RESULTS AND DISCUSSION

Initially, a numeric modal analysis was performed, for each model order, for comparison purposes. As the model order incerases, so does its capacity to model physical phenomena, and therefore the number of natural frequencies detected in a fixed frequency range will increase with the model order. In this evaluation, the range displayed goes from 1 to $50Hz$, and all frequencies detected in this range are displayed in Tab. 1. The first line is dedicated to the Timoshenko model (CBT), while the other lines correspond to the full 1_{st}, 2_{nd} and 3_{rd} order UF models, respectively. Additional natural frequencies were detected by the 3_{rd} order UF model, but only the repeated ones and those relevant to rotordynamics were presented.

Table 1: Natural frequencies detected by the different model orders ($\Omega = 0$)

CBT	44.71	44.71	-	26.12	26.12	23.80	-	-	-	-	-	5.76	5.80
UF 1_{st}	44.71	44.71	-	26.12	26.12	23.31	-	-	-	-	-	5.80	5.80
UF 2_{nd}	41.58	41.28	39.73	26.46	26.34	24.54	23.57	11.83	11.83	7.02	7.02	5.67	5.67
UF 3_{rd}	41.61	41.29	39.74	-	-	24.89	23.78	11.84	11.84	7.02	7.02	5.67	5.67

All values in [Hz].

A Campbell diagram was generated for the models, which as a waterfall plot, produced by obtaining the Frequency Response Function for the disks positions, along the directions x and z at a number of different Ω values. This mapping produces a better result than the standard Campbell representation for the higher order models, since they present results based on the relative amplitude of each natural frequency. In this manner, the relevant modes with high amplitude are in evidence, while the unimportant ones are kept to the background. Waterfall plots for the first disk in the vertical direction are presented in Figs. 2 through 5, for all models considered.

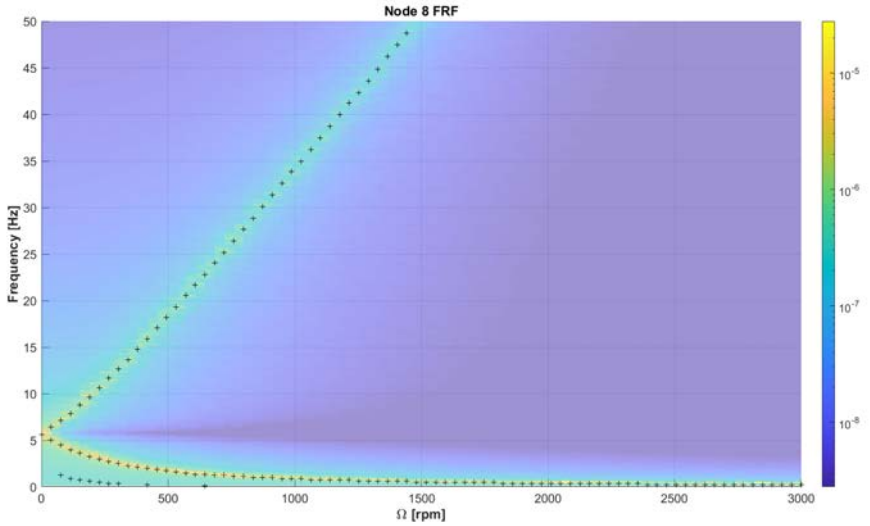

Figure 2: Timoshenko model unbalance response mapping - or Waterfall plot - captured for the first disk in the vertical direction. Scale in [m].

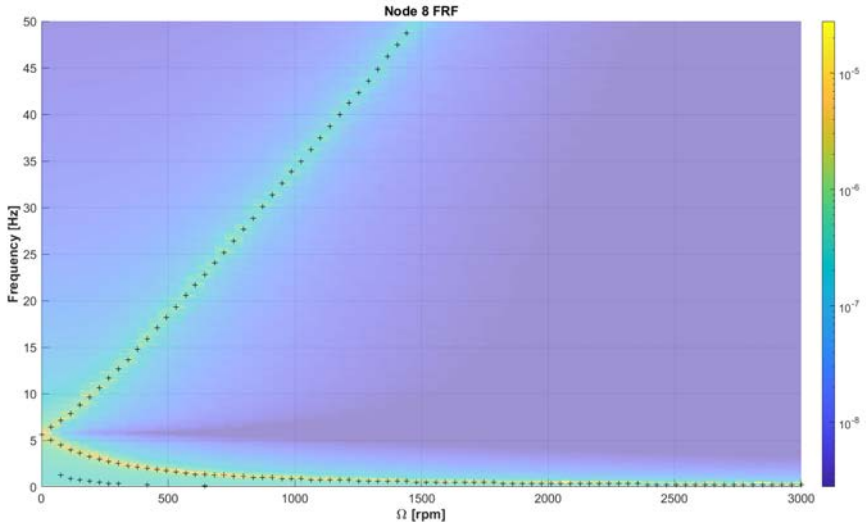

Figure 3: Complete first order UF model unbalance response mapping - or Waterfall plot - captured for the first disk in the vertical direction. Scale in [m].

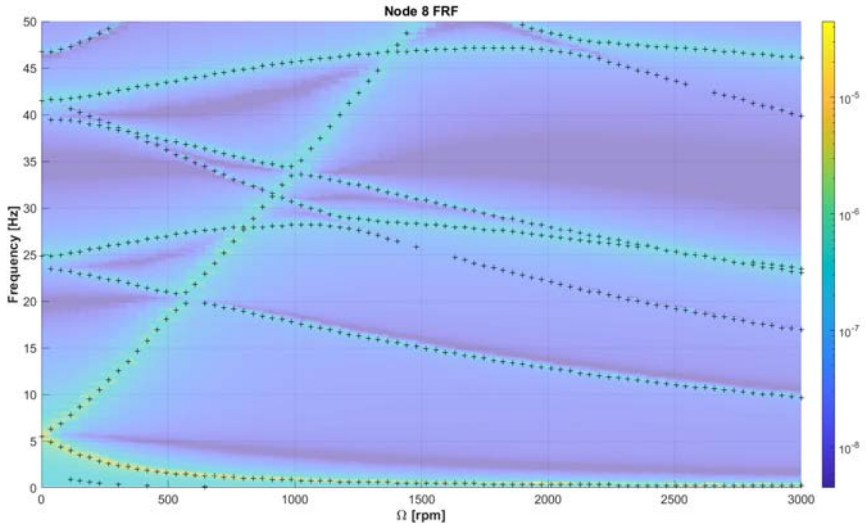

Figure 4: Complete second order UF model unbalance response mapping - or Waterfall plot - captured for the first disk in the vertical direction. Scale in [m].

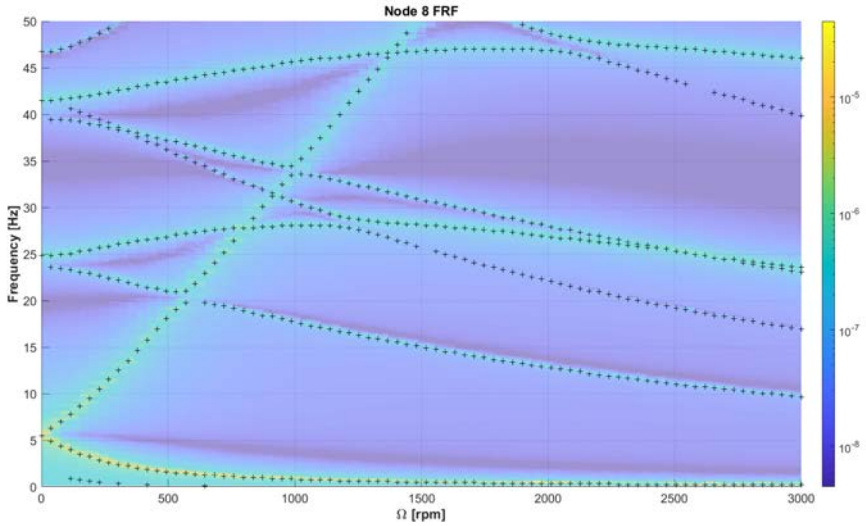

Figure 5: Complete third order UF model unbalance response mapping - or Waterfall plot - captured for the first disk in the vertical direction. Scale in [m].

Dynamic response analyses were performed to evaluate the model predictions for the transient behavior. A run-up analysis was simulated, from 0 to 3000 rpm, as can be seen in Fig. 6, and the displacement responses were obtained for the x and z directions on both disks nodes. While run-up tests, the implemented code runs a static simulation beforehand and uses its result as the initial condition for the running simulations, avoiding unphysical transient responses.

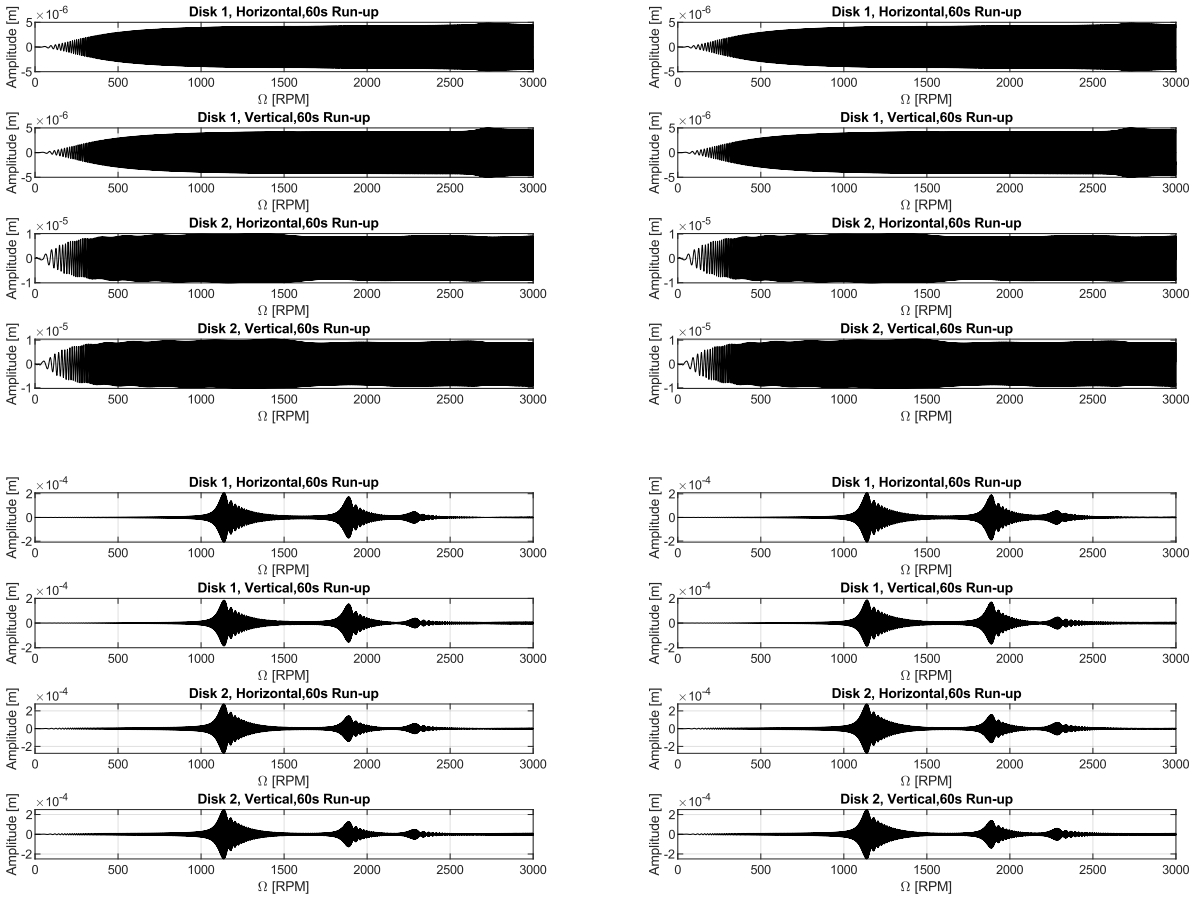

Figure 6: System runup response for multiple simulated models. Top left: 1st order UF degenerated into Timoshenko CBT; Top right: complete 1st order UF; Bottom left: complete 2nd order UF; Bottom right: complete 3rd order UF

6. CONCLUSIONS AND FUTURE ASPECTS

The UF model proposed was effectively implemented and improved, originating a very adaptable framework from which many new formulations, simplified and faster models can be developed. Introduction of new methodologies to represent specific details of composite materials, such as orthotropy and internal damping, were performed as intended. Once the core methodology to generate the element level matrices is in place, introducing new terms and functionalities is a relatively simple task, which is a great advantage when adapting pre-existing methodologies to new problems. In terms of computational performance, the code executes in similar speeds to its equivalents implemented using standard FEM methodologies. As no relevant difference was noted, no additional comparative tests were performed in this sense. As a proof of concept, our results demonstrated that the methodology is functional and efficient, assembling and solving the proposed problem, satisfactorily.

Analysing the responses obtained, in the order they were presented, one begins with the natural frequencies. An expected characteristic of the methodology is that the number of modes detected would increase with the order of the interpolation functions adopted, which is demonstrated by the results set. By using the CBT model, only four physical modes were detected with three of those being symmetric modes. Considering the complete first order UF, the same modes are found at almost the same frequency values, thus evidenciating the validity of using a CBT model (such as Timoshenko or Euler-bernoulli formulations) for slender shafts. Nevertheless, a great number of additional modes, including some symmetrical ones, were detected by increasing the order of interpolation to 2 and later on to 3. The frequency values of the already detected modes did not show considerable changes with the increment of the interpolation order. It is noteworthy that one of the symmetric modes (at roughly $26[Hz]$) was not detected by the third order UF, having been obtained by the other models. The third order UF has detected another 13 natural frequencies inside the studied frequency

range, and none of those have been previously detected nor were their symmetric counterparts.

Moving on to the FRF mappings - or Watterfall plots - one can notice great differences between the different interpolation orders. A simple Campbell diagram, as produced for the Timoshenko or complete first order UF, gives a better visualization than the Waterfall plots, due to the difference in relative amplitude between the different modes present in the system. For these cases, the natural frequencies are actually present, but with such a low relative magnitude that the detection threshold did not notice their presence. For this particular problem, a traditional Campbell was determined, and the Campbell diagram both for the Timoshenko model and the second order complete UF model are shown in Figs. 7 and 8. The diagrams for the first order UF and for the Timoshenko model are almost equivalent, and only the previous one is depicted in the present paper. In these diagrams it is evident the presence of the other natural frequencies, which were not detected in the Timoshenko waterfall plot.

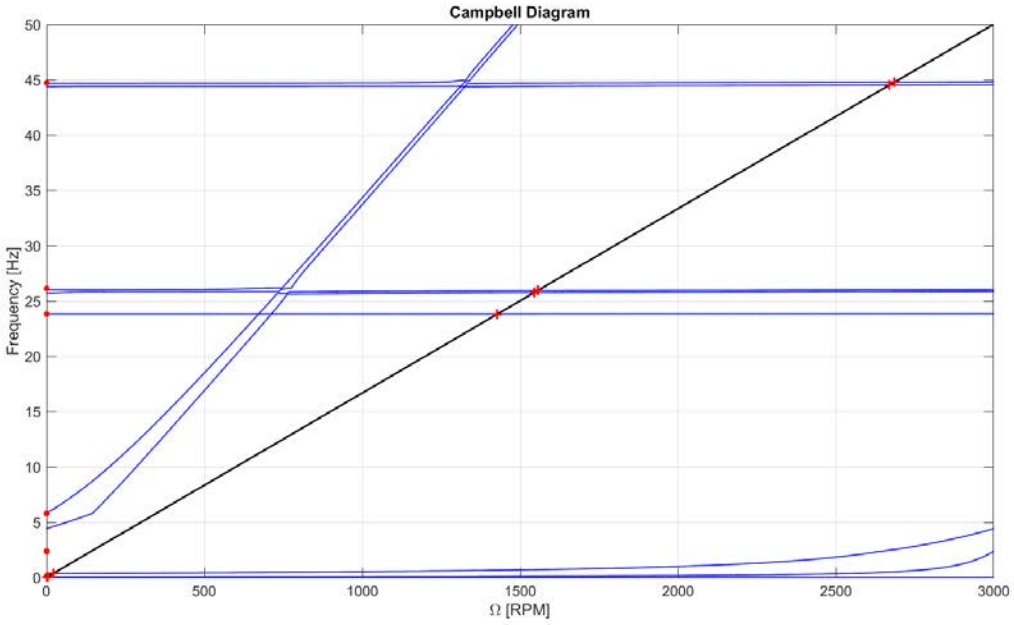

Figure 7: Campbell diagram for the Timoshenko model. In black, the 1X line is represented, the red dots give the frequency values determined by modal analysis ($at\ \Omega = 0$) and the red crosses mark the critical speeds

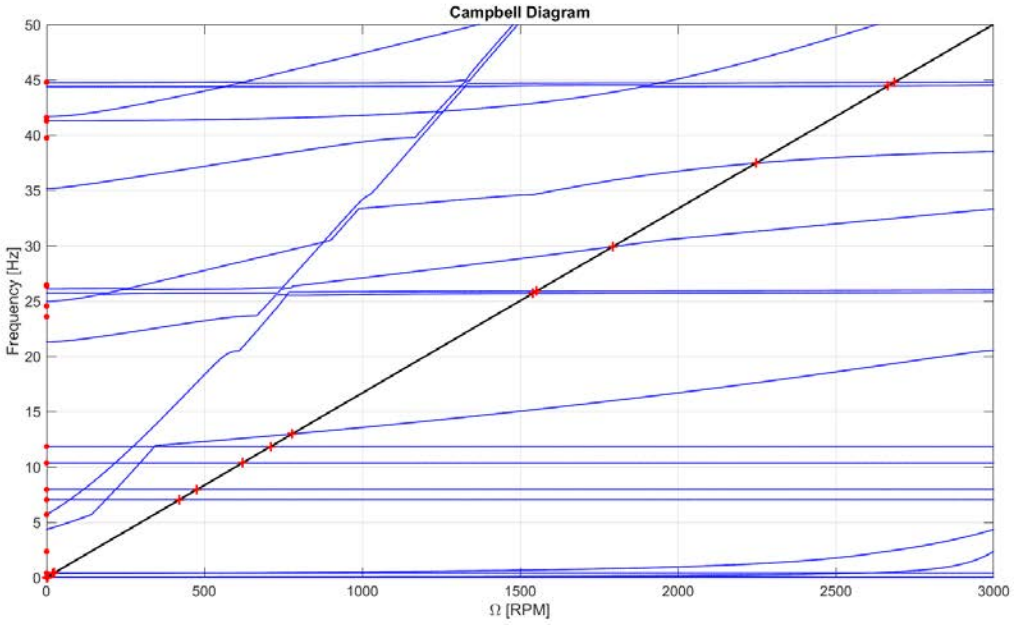

Figure 8: Campbell diagram for the complete second order UF model. In black, the 1X line is represented, the red dots give the frequency values determined by modal analysis ($at\ \Omega = 0$) and the red crosses mark the critical speeds

It is important to evaluate all available routes, for this is a preliminary study, and in this case it is evident that, for models of greater complexity than a CBT, the standard Campbell diagram is not adequate. Both representations, be it a Campbell or Waterfall plot, convey the same information, but presented in different forms. The interference between modes (veering) makes it quite difficult to individually isolate and track them in a Campbell diagram, and therefore the Waterfall plot is certainly a more appropriate method to map the system response in this cases. Specially for this task of tracking modes and for evaluating areas with multiple modes bundled together, the Waterfall plot appears to be an appropriate choice.

The final analysis performed is the run-up transient test, and in this evaluation all the previously discussed phenomena becomes apparent. For the Timoshenko and first order UF, it is clear that the critical frequencies are not adequately represented, and the reason for this is believed to be the absence of cross-coupled terms in those models. However, when observing the results for the second and third order UF models it becomes evident that the response is qualitatively accurate, and resembles what is expected from experimental results. The system response exponentially increases and then decreases when crossing critical frequencies; the beating phenomena is observed in the exponential decay regions. Also, different amplitudes are noticed between the vertical and horizontal directions, evidenciating the gravity force influence on the overall dynamics of the model. This behavior is observed because even if the bearings are considered symmetric, the shaft structure itself is a composite, which inherently couples the cross-section x and z directions.

In this study the analyses were focused on the natural frequencies that are relevant for rotordynamics. However, an additional evaluation to reconstruct and plot the mode shapes is being developed and, due to both time and space constraints, will be presented in future publications. The proposed procedure to reconstruct the mode shapes involves reassembling the DoF displacement solutions into physical coordinates, in a generalized manner. Ideally, it would give certainty to the interpretations about each natural frequency and associated vibration mode detected, highlighting the extra modes presented by the higher order models.

According to the results presented, the greater order of interpolation, and consequently the model complexity, the better the response similarity to real systems dynamics. An evident drawback is the increased computational cost which, given the nature of this methodology, can be easily reduced by identifying and neglecting the irrelevant terms for any given application.

7. ACKNOWLEDGMENTS

The authors are thankful for the financial support provided to the present research effort by CNPq (574001/2008-5,304546/2018-8, and 431337/2018-7), FAPEMIG (TEC-APQ-3076-09, TEC-APQ-02284-15, TEC-APQ-00464-16, and PPM-00187-18), and CAPES through INCT-EIE and PDSE scholarship (88881.187110/2018-01).

8. REFERENCES

Barbosa, P.C.P.F., Cavalini Jr., A.A. and Steffen Jr., V., 2018. *Analysis of the dynamic behavior of composite shafts on rotating machines*. Ph.D. thesis, Universidade Federal de Uberlândia, Uberlândia, Brasil.

Barbosa, P.C.P.F., Del Claro, V.T.S., Sousa Jr., M.S., Cavalini Jr., A.A. and Steffen Jr., V., 2019. "Shbt based modeling of a composite hollow shaft regarding its dynamic behavior prediction". In *Proceedings of SIRM 2019 – 13th International Conference on Dynamics of Rotating Machines*. Copenhagen, Denmark.

Brush, M., 1999. "Still spinning after all these years: A profile of the ultracentrifuge". *The Scientist*, Vol. 13, pp. 16–18.

Bucciarelli, L.L., 1982. "On the instability of rotating shafts due to internal damping". *Journal of Applied Mechanics*, Vol. 49, pp. 425–428.

Carrera, E. and Filippi, M., 2015. "Vibration analysis of thin/thick, composites/metallic spinning cylindrical shells by refined beam models". *ASME. J. Vib. Acoust*, Vol. 137, pp. 031020–1.

Carrera, E., Giunta, G. and Petrolo, M., 2011. *Beam Structures: Classical and Advanced Theories*. John Wiley & Sons, New Jersey, 1st edition.

Carrera, E., Giunta, G., Petrolo, M. and Zappino, E., 2014. *Finite Element Analyses of Structures Through Unified Formulation*. John Wiley & Sons, New Jersey, 1st edition.

Cavalini Jr., A.A., aes, T.G., Da Silva, B.R.M.G. and Steffen Jr., V., 2017. "Analysis of the dynamic behavior of a rotating composite hollow shaft". *Latin American Journal of Solids and Structures*, Vol. 14, pp. 1–16.

Del Claro, V.T.S., Barbosa, P.C.P.F., Cavalini Jr., A.A. and Steffen Jr., V., 2017. "A shell based fem model for thick walled composite rotors". In *Proceedings of the 24th ABCM COBEM*. Curitiba, Brazil.

Filippi, M., 2015. *A variable kinematic one-dimensional model for aeroelasticity and dynamic analysis of multi-layered rotors*. Ph.D. thesis, Politecnico di Torino, Turin, Italy.

Friswell, M.I., Penny, E.T., Garvey, D. and Lees, W., 2010. *Dynamics of Rotating Machines*. Cambridge University Press, Cambridge, 1st edition.

Gubran, H.B.H. and Gupta, K., 2005. "The effect of stacking sequence and coupling mechanisms on the natural frequencies of composite shafts". *Journal of Sound and Vibrations*, pp. 231–248.

Gupta, K., 2015. "Composite shaft rotor dynamics: An overview". In *Proceedings of Vibration Engineering and Technology of Machinery - Vetomac X*. Manchester, England.

Meirovitch, L., 1980. *Computational Methods in Structural Dynamics*. Sijtihoff and Nordhoff International Publishers B. V., Alpen aan den Rijn, The Netherlands, 1st edition.

Mendonça, W.R.P., Medeiros, E., Pereira, A.L.R. and Mathias, M.H., 2017. "The dynamic analysis of rotors mounted on composite shafts with internal damping". *Composite Structures*, pp. 50–62.

Silveira, M.E., 2001. *Analise Do Comportamento Dinamico De Rotores Em Eixos Bobinados*. Ph.D. thesis, Federal University of Santa Catarina, Florianopolis, Brazil.

Singh, S.P. and Gupta, K., 1996. "Composite shaft rotordynamic analysis using a layerwise theory". *Journal of Sound and Vibration*, pp. 739–756.

Sino, R., 2007. *Comportement Dynamique Et Stabilite Des Rotors: Application Aux Rotors Composites*. Ph.D. thesis, Insa Lyon, Lyon, France.

Sino, R., Baranger, A.B. and Jacquet, A.G., 2008. "Dynamic analysis of a rotating composite shaft". *Composites Science and Technology*, p. 337–345.

Tsai, S.W., 1998. *Composites Design*. Dayton, Ohio, USA, 4th edition.

Wasilkoski, C.M., 2006. *Mechanical Behavior of Composite Materials*. Ph.D. thesis, UFPR, Curitiba, Brasil.

Zienkiewicz, O.C. and Taylor, R.L., 2005. *The Finite Element Method for Solid and Structural Mechanics*. Elsevier, New York, 5th edition.